NAVIGATION, the Journal of the Institute of Navigation
Accepted for publication, July 2012

Self-Contained Antenna Array Calibration using GNSS Signals

Pratibha B Anantharamu, Daniele Borio and Gérard Lachapelle
Position, Location And Navigation (PLAN) group,
Department of Geomatics Engineering, University of Calgary, Canada

ABSTRACT

Antenna array processing techniques require calibration algorithms that often rely on the availability of signal sources at known locations, a good knowledge of the array manifold or a reference antenna. An alternative is provided by GNSS signals that provide the location of their sources as part of their navigation data. In this paper, a projection methodology using GNSS signals is proposed for the calibration of antenna arrays. The Gram Schmidt process is used along with the properties of the signal steering vectors to determine linear relationships between the recovered signals and the calibration parameters. The obtained system of equations is then solved in the Minimum Mean Square Error (MMSE) sense leading to the estimated calibration parameters. The proposed algorithm accounts for signal gain/phase mismatches and mutual coupling between array elements.

Finally, the effectiveness of the proposed technique and its suitability for beamforming and Direction-of-Arrival (DoA) applications is supported by several experiments performed using live GPS signals and a GNSS software receiver.

INTRODUCTION

The continuously evolving Global Navigation Satellite System (GNSS) technology is moving towards the development of receivers equipped with several antennas. The use of an antenna array [1] provides enhanced performance such as improved signal quality and

detectability, anti-jamming, interference rejection and improved multipath mitigation compared to single antenna techniques. Antenna arrays are capable of steering their beam pattern towards desired directions to maximize the signal-to-interference-plus-noise ratio and cancel co-channel interference from particular directions.

One of the main challenges faced while using antenna arrays is their calibration. Signals received from different array sensors suffer from additional phase shifts due to antenna mutual coupling, antenna gain/phase mismatches, antenna phase centre variations and distortions introduced by different Radio Frequency (RF) front-ends along with phase offsets due to the antenna array structure. In addition, environmental parameters such as temperature can influence the overall gain and phase response of an antenna array. A perfect knowledge of the array manifold including these kinds of variations is not available in practice. Calibration compensates the combined effect of unknown antenna phase, gain and mutual coupling which would degrade the performance of array processing algorithms if not addressed.

For effective array processing, calibration becomes one of the vital processes to be performed before combining the signals from the array. Thus, the design of robust calibration algorithms that corrects for gain/phase mismatches among array data becomes a necessity. Several techniques based on the availability of signals transmitted from known locations have been proposed in the literature [2, 3]. These methodologies are based on the maximum likelihood and least squares approaches and requires a good knowledge of the received signals. More specifically, the amplitude of the received signals is assumed known and their phase perfectly recovered during the down-conversion process. This assumption was justified by the fact that, in the considered cases, calibration was performed in a

controlled environment using dedicated signal sources. This assumption is relaxed in this paper and an algorithm independent from the received signal amplitude/phase is proposed.

Antenna array calibration algorithms require reference signal sources in known locations. GNSS receivers are capable of providing the satellite locations with a meter level accuracy that is sufficiently good for calibration algorithms. Calibration of antenna arrays using GNSS signals have been proposed in [4, 5]. A seven element custom array was calibrated for antenna gain/phase mismatches using a least squares approach applied on the GPS correlator outputs in [4]. In [5], a procedure to obtain the array manifolds of GNSS antennas using Space-Time Adaptive Processing (STAP) was proposed. In this procedure, the STAP weights were updated in order to maximize the cross-correlator outputs; in a second step, the array manifold was determined in the least squares sense. Although [4] and [5] suggested the use of GNSS signals for the calibration of the antenna array, different signal models and target applications were considered. In order to reach the targeted level of accuracy, additional hardware such as a reference antenna and an inertial navigation unit were also required.

In this paper, a calibration algorithm based on the availability of GNSS signals is proposed. The main objective is to obtain a calibration technique not requiring any additional equipment than the already available GNSS signals. A least squares solution based on a projection methodology is used to determine the calibration parameters. The main idea behind the technique is to obtain a linear relationship between the calibration parameters and the observed correlator outputs. This relationship has to be independent from relative satellite signal amplitude and phase differences. This is achieved by projecting the correlator outputs from the array data onto the steering vector null space.

In a second stage, the calibration parameters are estimated by solving the obtained linear system in the least squares sense.

The proposed calibration technique exploits the orthogonal projection principle already adopted by algorithms such as the multiple signal classification (MUSIC) [6] and subspace optimization technique [7]. The MUSIC algorithm estimates the Direction of Arrival (DoA) of incident signals by exploiting the orthogonality between signal and noise subspaces. The noise subspace is identified using the eigen-decomposition of the received signal covariance matrix which is used in the determination of desired signals. In the subspace optimization technique [7], a calibration algorithm based on the minimization of a cost function is proposed. The cost function is based on the scalar product of the actual array response and orthogonal vectors obtained as the eigenvectors of the noise correlation matrix. Thus, in these techniques, the covariance matrix of the incoming signals is assumed to be known. This stringent requirement is no longer necessary in the proposed technique that allows array calibration without any additional knowledge on the received GNSS signals. This methodology essentially differs from the above mentioned techniques since it does not rely on the knowledge of the signal/noise correlation matrices.

The effectiveness of the proposed technique is demonstrated through several experiments conducted using a GSS7700 Spirent GPS Hardware Simulator, capable of simulating two antennas, and live GNSS signals. Antenna positions, beam pattern and satellite signal levels were configured according to different specifications.

Intermediate Frequency (IF) data were collected using two different hardware systems able to recover samples from different antennas. At first a National Instruments (NI) PXI-

5661 [8] vector analyzer was used to synchronously collect data from the two RF outputs of the simulator. Although driven by the same clock, the front-ends of the NI system employ different Phase Lock Loops (PLLs) for the signal down-conversion. This introduces progressive phase shifts among signals from different front-ends. This problem has been solved by using a pilot tone and including a phase compensation block in the calibration algorithm. It is noted that this part of the algorithm is not required if a common PLL is used for the down-conversion of all the recovered signals. The NI system was not designed for array processing and its use was adopted to stress the capability of the proposed algorithm that effectively enables multi-antenna processing even in such unfavourable conditions.

A second data collection system, capable of synchronously collecting data from up to 4 antennas, was also adopted for testing the proposed calibration algorithm. The data collection system was developed in the PLAN Group at the University of Calgary and it is an extension of the single channel front-end detailed in [9]. In this case, all the front-ends integrated in the data acquisition system adopt the same PLL for the signal down-conversion and thus relative phase shifts do not occur.

Real data from GPS satellites have been collected using up to four antennas placed in various positions to form a planar/triangular array structure with different antenna spacing. It is noted that no effort were made to limit mutual coupling with proper antenna integration. The antennas used for the experiments are commercially available and designed for standalone operations. In this way, particularly critical conditions were obtained.

A modified version of the University of Calgary software receiver, GSNRx^{TM} [10], has been used to simultaneously process multi-antenna data and produce synchronous correlator outputs. These correlator outputs were fed to the proposed calibration algorithm and a good match between the ideal and calibrated array beam pattern was observed. This work is an extension of the conference paper [11] that provided results only for simulated data. In this paper, a more detailed description of the calibration methodology along with results obtained using live GPS signals is provided. Beamforming results after applying the proposed projection based calibration methodology on a real planar array are also provided.

The remainder of this paper is organized as follows: The second section introduces the signal and system model used for the development of antenna array calibration technique. The tracking structure adopted for the antenna array processing is also discussed. Section 3 derives the proposed projection methodology for array calibration. Simulation results and real data analysis are detailed in Section 4. Finally, some conclusions are drawn in Section 5.

SIGNAL MODEL

The complex baseband signal received by a single antenna GNSS receiver in the absence of multipath signals can be modeled as

$$\begin{aligned} x(t) &= \sum_{i=0}^{L-1} y_i(t) + \eta(t) \\ &= \sum_{i=0}^{L-1} A_i d_i\left(t-\tau_{0,i}\right) c_i\left(t-\tau_{0,i}\right) \exp\left\{ j\left(2\pi f_{0,i} t + \phi_{0,i}\right)\right\} + \eta(t) \end{aligned} \tag{1}$$

which is the sum of L useful components, coming from L different satellites, and a noise term, $\eta(t)$. A_i is the amplitude of the i^{th} signal component, $f_{0,i}$ and $\phi_{0,i}$ its Doppler frequency and carrier phase. $c_i(\cdot)$ is the ranging code used to spread the navigation data, $d_i(\cdot)$, whereas $\tau_{0,i}$ denotes the code delay introduced by the communication channel on the i^{th} useful component. The hypothesis of multipath absence is common in the literature [4] and it is used to simplify the calibration procedure.

When considering antenna arrays, the effect of closely spaced antennas on the received signal, $x(t)$, needs to be considered. Consider an array of M elements on a plane with a single signal source (GNSS satellite) as shown in Figure 1. Under ideal conditions, the relative phase between signals received from different antennas can be expressed as a function of the vector wave number

$$\mathbf{k} = \frac{2\pi}{\lambda}\left[\cos\varepsilon\sin\alpha \quad \cos\varepsilon\cos\alpha \quad \sin\varepsilon\right]^{\mathrm{T}} \tag{2}$$

where ε and α are the elevation angle and azimuth angle of the signal source defined with respect to a triplet of orthogonal axes as shown in Figure 1. λ denotes the wave-length of the signal carrier.

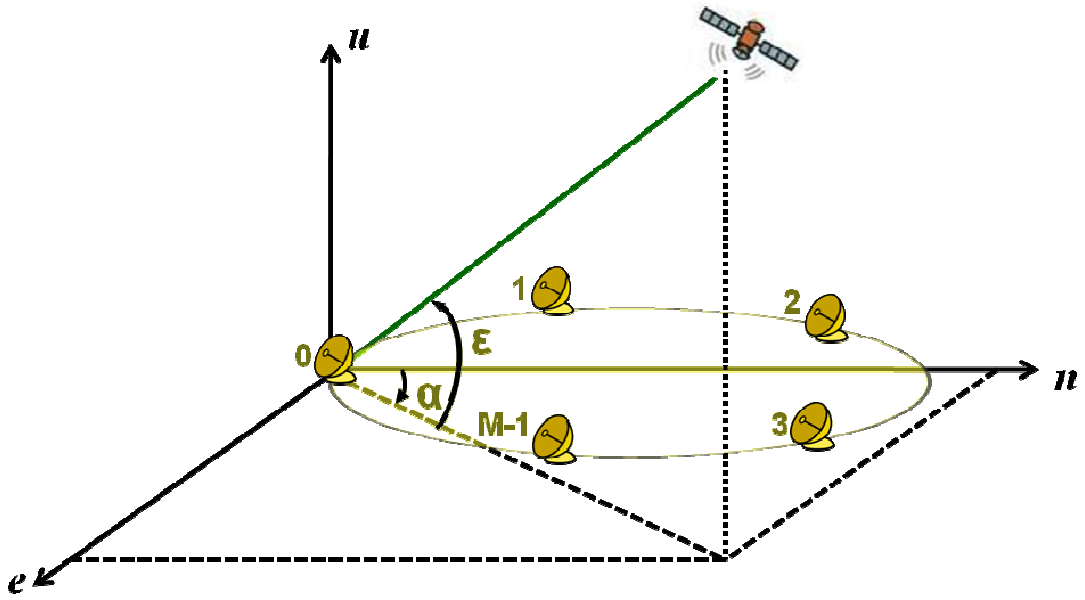

Figure 1 Schematic representation of an antenna array receiving a single signal from a source at a specific elevation and azimuth.

Each antenna element receives a copy of the useful signal with a different phase defined by the complex steering vector that can be expressed as

$$\begin{aligned}\mathbf{s}(\varepsilon,\alpha) &= \begin{bmatrix} s_0 & s_1 & s_2 & \dots & s_{M-1} \end{bmatrix}^{\mathbf{T}} \\ &= \begin{bmatrix} 1 & \exp\{-j\mathbf{k}^{\mathbf{T}}\mathbf{r_1}\} & \exp\{-j\mathbf{k}^{\mathbf{T}}\mathbf{r_2}\} & \cdots & \exp\{-j\mathbf{k}^{\mathbf{T}}\mathbf{r_{M-1}}\} \end{bmatrix}^{T}\end{aligned} \tag{3}$$

where $\mathbf{r}_m = \begin{bmatrix} e_m & n_m & u_m \end{bmatrix}$ is the vector defining the position of the m^{th} antenna. The first element of the antenna is placed in the centre of the coordinate system justifying the fact that $s_0 = 1$. In (1), L GNSS signals are received from L different directions and a different steering vector is associated to each useful component. Thus, under ideal conditions, the vector of the signals received by the antenna array can be approximately modeled as

$$\mathbf{x}(t) = \begin{bmatrix} x_0(t) \\ x_1(t) \\ \vdots \\ x_{M-1}(t) \end{bmatrix} = \sum_{i=0}^{L-1} \mathbf{s}_i y_i(t) + \mathbf{n}(t) \tag{4}$$

where $\mathbf{s}_i = \begin{bmatrix} s_{i,0} & s_{i,1} & \cdots s_{i,M-1} \end{bmatrix}^T$ denotes the steering vector associated to the i^{th} GNSS signal. $\mathbf{n}(t) = \begin{bmatrix} \eta_0(t) & \eta_1(t) & \cdots & \eta_{M-1}(t) \end{bmatrix}^T$ is the vector of the noise components observed by the M antennas. The components of $\mathbf{n}(t)$ are assumed independent since they are mainly due to different front-ends and hardware paths. An index has been added to indicate signals from a specific antenna.

Eq. (4) represents the model of the signals received by an ideal antenna array where the different location of the sensor only introduces a fixed additional phase in the received signals. This model is simplistic and neglects the effects of mutual coupling [12] and gain/phase mismatches among different array elements. Mutual coupling is due to the fact that antennas reradiate parts of their received signals that are recovered by the other elements of the array. Gain and phase mismatches make different antennas observe different signal amplitudes and phases. Thus, the signal received by the m^{th} antenna can be modeled as a linear combination of the signals received by all the array elements as

$$\tilde{x}_m(t) = \sum_{k=0}^{M-1} \sum_{i=0}^{L-1} w_{m,k} s_{i,m} y_i(t) + \eta_m(t) \tag{5}$$

where the symbol ~ is used to denote quantities affected by the presence of mutual coupling and amplitude/phase mismatches. $w_{m,k}$ is a complex weight determining the impact of the signal from the k^{th} antenna on the m^{th} array element. In the following, it is

assumed that $w_{m,k}$ does not depend on the direction of arrival of the i^{th} signal. Thus, (5) can be written in matrix form as

$$\tilde{\mathbf{x}}(t) = \begin{bmatrix} \tilde{x}_0(t) \\ \tilde{x}_1(t) \\ \vdots \\ \tilde{x}_{M-1}(t) \end{bmatrix} = \sum_{i=0}^{L-1} \mathbf{C}\mathbf{s}_i y_i(t) + \mathbf{n}(t) \tag{6}$$

where

$$\mathbf{C} = \begin{bmatrix} w_{0,0} & w_{0,1} & \cdots & w_{0,M-1} \\ w_{1,0} & w_{1,1} & \cdots & w_{1,M-1} \\ \cdots & \cdots & \cdots & \cdots \\ w_{M-1,0} & w_{M-1,1} & \cdots & w_{M-1,M-1} \end{bmatrix} \tag{7}$$

is a $M \times M$ matrix containing the coefficients $w_{m,k}$. $\mathbf{C}$ is assumed full-rank and calibration is defined as the process of estimating the coefficients of $\mathbf{C}$ and inverting the effects of mutual coupling and amplitude/phase mismatches.

It is noted that the coefficients of $\mathbf{C}$ are time-varying and depend on the satellite scenario. Calibration should thus be performed at regular time intervals. These changes are however slow and $\mathbf{C}$ can be considered constant during the duration of the experiments described in the following sections. For this reason, the problem of updating $\mathbf{C}$ is not further considered in this paper.

The correlation process

GNSS signals are usually buried in noise and de-spreading operations are required to boost the signal power and isolate the different signal components. More specifically, the spreading sequences, $c_i(t)$, are from a family of quasi-orthogonal codes that allow the

independent processing of each signal component. De-spreading is achieved by correlating the input signal $\tilde{x}_m(t)$ with a locally generated replica of the i^{th} GNSS signal [13]. In the correlation process, the carrier of the incoming signal is at first wiped off using a local complex carrier replica that brings the signal to baseband. The spreading code is also wiped off using a ranging code generator [13]. The signal obtained after carrier and code removal is integrated and dumped (I&D) over T seconds.

The correlator output obtained considering the signal from the m^{th} antenna and with the h^{th} local code can be modeled as

$$\begin{aligned} q_{m,h} &= \frac{1}{T}\int_0^T \tilde{x}_m(t)c_h\left(t-\tau_h\right)\exp\left\{-j\left(2\pi f_{D,h}t+\phi_h\right)\right\}dt \\ &= \frac{1}{T}\int_0^T \sum_{k=0}^{M-1}\sum_{i=0}^{L-1} w_{m,k}s_{i,m}y_i(t)c_h\left(t-\tau_h\right)\exp\left\{-j\left(2\pi f_{D,h}t+\phi_h\right)\right\}dt+\bar{\eta}_{m,h} \\ &= \sum_{k=0}^{M-1}\sum_{i=0}^{L-1} w_{m,k}s_{i,m}\frac{1}{T}\int_0^T y_i(t)c_h\left(t-\tau_h\right)\exp\left\{-j\left(2\pi f_{D,h}t+\phi_h\right)\right\}dt+\bar{\eta}_{m,h} \\ &\approx \sum_{k=0}^{M-1} w_{m,k}s_{h,m}\frac{1}{T}\int_0^T y_h(t)c_h\left(t-\tau_h\right)\exp\left\{-j\left(2\pi f_{D,h}t+\phi_h\right)\right\}dt+\bar{\eta}_{m,h} \\ &= \sum_{k=0}^{M-1} w_{m,k}s_{h,m}A_hR\left(\Delta\tau_h\right)\frac{\sin\left(\pi\Delta f_hT\right)}{\pi\Delta f_hT}\exp\left\{j\pi\Delta f_hT+j\Delta\phi_h\right\}+\bar{\eta}_{m,h} \end{aligned} \tag{8}$$

where

- τ_h is the delay estimate provided by the receiver for the h^{th} signal component and $\Delta\tau_h=\tau_{0,h}-\tau_h$ is the code delay error;
- $f_{D,h}$ is the Doppler frequency estimated by the receiver for the h^{th} signal component and $\Delta f_{D,h}=f_{0,h}-f_{D,h}$ is the Doppler frequency error;
- ϕ_h is the estimated carrier phase and $\Delta\phi_h=\phi_{0,h}-\phi_h$ is the residual phase error;
- $R(\cdot)$ denotes the correlation function of the ranging code;
- $\bar{\eta}_{m,h}$ is a Gaussian random variable obtained by processing $\eta_m(t)$ using the h^{th} local signal. In the following, $\bar{\eta}_{m,h}$, for $m=0,...,M-1$ and $h=0,...,L-1$ are

assumed to be zero mean independent identically distributed (i.i.d) complex random variables. The real and imaginary parts of $\overline{\eta}_{m,h}$ are independent with variance σ_{η}^{2}.

In (8), the impact of the navigation message, that is assumed constant during the integration interval, T, is neglected. In the following, it is assumed that $\Delta\tau_h \approx 0$ and $\Delta f_{D,h} \approx 0$, implying

$$q_{m,h} = \sum_{k=0}^{M-1} w_{m,k} s_{h,m} A_h \exp\{ j\Delta\phi_h \} + \overline{\eta}_{m,h}. \tag{9}$$

The delay, frequency and phase estimates can be obtained using the processing structure shown in Figure 2. The signal from the first antenna is tracked using a standard PLL and Delay Lock Loop (DLL) [13]. Signals from the other array elements are tracked using the Doppler frequency, carrier phase and code delay provided by the DLL and PLL locked on the first signal. It is noted that the choice of using the first antenna is arbitrary (any other antennas can be used) and does not imply that calibration is performed with respect to the first antenna. This type of processing is required in order not to introduce additional relative delays and carrier phases among signals from different antennas.

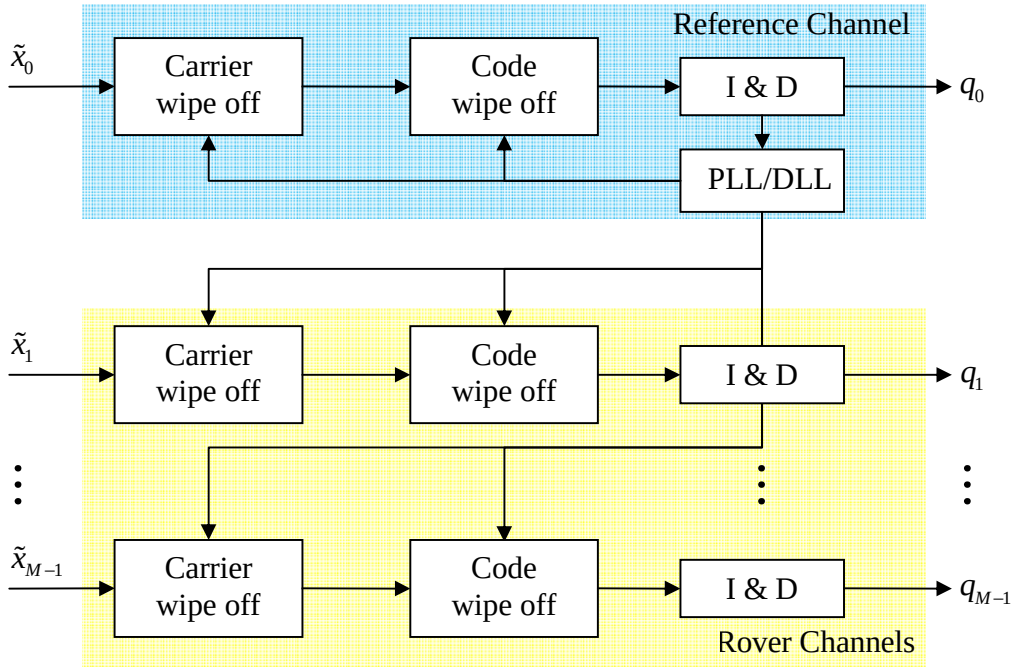

Figure 2 GNSS signal tracking structure for multi-antenna processing. The same local carrier and code are used for processing different signals, preserving the amplitude/phase relationship among different signal components.

Using the same local signal replica for the de-spreading of the signals from different antennas, it is possible to write the vector of the correlator outputs for the h^{th} spreading code as

$$\mathbf{q}_h = \begin{bmatrix} q_{0,h} \\ q_{1,h} \\ \vdots \\ q_{M-1,h} \end{bmatrix} = \mathbf{C}\mathbf{s}_h A_h \exp\{j\Delta\phi_h\} + \begin{bmatrix} \bar{\eta}_{0,h} \\ \bar{\eta}_{1,h} \\ \vdots \\ \bar{\eta}_{M-1,h} \end{bmatrix}. \tag{10}$$

Eq. (10) is the basic equation that will be used in the next section to derive a calibration methodology based on the availability of GNSS signals. It is noted that GNSS signals continuously broadcast the position of their sources. In addition to this, a rough estimate

of the user position can be determined using, for example, the signal from a single antenna. The position of a reference antenna, the array orientation and satellite positions allow the computation of the steering vectors that can be assumed known. The array orientation is required to determine the position of the different array sensors and compute the vectors $\mathbf{r}_m$ introduced in Eq. (3). The antenna orientation can be obtained by aligning the array along a known direction or it can be estimated using attitude determination methods available from the literature [14]. The determination of the antenna orientation is out of the scope of this paper. In the next section, a calibration methodology based on the availability of GNSS signals is proposed.

PROJECTION BASED CALIBRATION METHODOLOGY

In (10), the effect of relative amplitude and phase variations among different satellite signals, A_h and $\Delta\phi_h$, are unknown and can be considered as nuisance parameters during the estimation of the coefficients of the calibration matrix. This section details the methodology proposed to estimate the calibration parameters independently from the relative satellite signal amplitude and phase values.

For each satellite steering vector, $\mathbf{s}_h$, it is possible to determine $M-1$ orthogonal vectors using for example the Gram–Schmidt process [15]. These vectors, denoted by $\mathbf{h}_{k,h}$, satisfy the following property:

$$\mathbf{h}_{k,h}^{H} \cdot \mathbf{s}_h = 0, \quad \text{for } k = 0,...,M-2 \tag{11}$$

where $(\cdot)^H$ denotes Hermitian transpose. Property (11) is preserved through multiplication by a complex constant:

$$\mathbf{h}_{k,h}^{H} \cdot \mathbf{s}_h A_h \exp\{ j\Delta\phi_h \} = 0, \quad \text{for } k = 0,...,M-2. \tag{12}$$

Collecting the $M-1$ orthogonal vectors in a single matrix, H_h, leads to the following condition

$$\mathbf{H}_h^{H} \cdot \mathbf{s}_h A_h \exp\{ j2\pi\Delta\phi_h \} = \mathbf{0} \tag{13}$$

where

$$\mathbf{H}_h = \left[\mathbf{h}_{0,h} \quad \mathbf{h}_{1,h} \quad \cdots \quad \mathbf{h}_{M-2,h} \right]. \tag{14}$$

The columns of the matrix $\mathbf{H}_h$ define the null space of the steering vector $\mathbf{s}_h$. It is noted that the projection (14) is independent from the amplitude/phase of the complex correlators, $A_h \exp\{ j\Delta\phi_h \}$, and thus can be used for obtaining linear equations for determining $\mathbf{C}$, the calibration matrix. More specifically, by neglecting the impact of noise, the following conditions can be imposed

$$\mathbf{H}_h^{H} \mathbf{C}^{-1} \mathbf{q}_h = \mathbf{0} \quad \text{for } h = 0,1,...,L-1. \tag{15}$$

The inverse of the calibration matrix, $\mathbf{C}^{-1}$, will be denoted as

$$\mathbf{C}^{-1} = \mathbf{A} = \begin{bmatrix} a_{0,0} & a_{0,1} & \cdots & a_{0,M-1} \\ a_{1,0} & a_{1,1} & \cdots & a_{1,M-1} \\ \cdots & \cdots & \cdots & \cdots \\ a_{M-1,0} & a_{M-1,1} & \cdots & a_{M-1,M-1} \end{bmatrix} \tag{16}$$

and conditions (15) will be used to determine its coefficients, $a_{i,j}$.

As already pointed out, (15) is preserved through complex multiplication. Thus, $\mathbf{A}$ can be univocally determined only by imposing a normalization condition on its coefficients. The convention

$$\mathrm{a}_{0,0} = 1 \tag{17}$$

is adopted here and used to transform (15) into linear equations. More specifically, a single condition from (15) can be written as

$$\begin{aligned}\mathbf{h}_{k,h}^{H}\mathbf{C}^{-1}\mathbf{q}_h &= \mathbf{h}_{k,h}^{H}\mathbf{A}\mathbf{q}_h \\ &= \sum_{i=0}^{M-1}\sum_{j=0}^{M-1} h_{k,h,i}^{*} a_{i,j} q_{j,h} = h_{k,h,0}^{*} q_{0,h} + \sum_{i\neq 0,\, j\neq 0} a_{i,j} h_{k,h,i}^{*} q_{j,h} \\ &= b_{k,h} + \sum_{i\neq 0,\, j\neq 0} a_{i,j} b_{k,h}^{i,j} = 0\end{aligned} \tag{18}$$

where $b_{k,h} = h_{k,h,0}^{*} q_{0,h}$ and $b_{k,h}^{i,j} = h_{k,h,i}^{*} q_{j,h}$.

Eq. (18) defines a linear equation in $M^2 - 1$ unknowns. When L satellites are in view $L(M-1)$ equations can be found and the matrix $\mathbf{A}$ can be determined when $L \geq M+1$. If $L > M+1$, the system of equations defined by (18) can be solved in the least squares sense [16]. The calibration procedure based on the projection methodology described above is summarized in Algorithm 1. The matrix $\mathbf{A}$ can be used to compensate the effects of mutual coupling and apply beamforming and angle-of-arrival estimation algorithms.

Data : The signal vector $\tilde{x}(t)$
Result : Estimate of the inverse of the calibration matrix, $\mathbf{A} = \mathbf{C}^{-1}$
begin
1) Compute the correlator outputs, $\mathbf{q}_h$ using a common signal replica
2) Determine the steering vectors, $\mathbf{s}_h$
3) **for** *each steering vector*, $\mathbf{s}_h$, $h = 0,1,...,L-1$ **do**
   Use the Gram–Schmidt process to determine the orthogonal vectors, $\mathbf{h}_{k,h}$
   Use (18) to determine linear equations in the coefficients of $\mathbf{A}$
end
4) Solve the linear system and determine $\mathbf{A}$.
End

Algorithm 1 Procedure for the estimation of the inverse of the calibration matrix, A.

RESULTS AND ANALYSIS

In this section, the proposed projection methodology for antenna array calibration is analyzed for different array structures, number of antenna elements and satellite constellation. Monte Carlo simulations have been at first used to determine the impact of the integration time on the estimated calibration parameters. The results have then been used for the processing of hardware simulated and real GPS signals. A standard beamforming [17] algorithm has been implemented to test the effectiveness of the proposed calibration technique.

Monte Carlo analysis

A Monte Carlo approach [18] has been used for the analysis of the proposed methodology where model (10) was directly simulated for different satellites and antenna array configurations. A constellation of ten satellites with elevation angles ranging from 10 to 90 degrees was simulated and correlator outputs were generated in order to match input C/N_0 values varying in the 30-50 dB-Hz range [19]. Calibration matrices with coefficients selected in a random way, using a complex Normal distribution, were used to simulate mutual coupling and amplitude/phase mismatches. A sample result of this analysis is shown in the following. The performance of the calibration algorithm has been analyzed as a function of the integration time, T, required to obtain the correlator outputs for a five element linear array with inter-antenna spacing equal to $\lambda/2$. The mean phase square error (MSE) for different T using the projection based calibration methodology is shown in Figure 3. For the calibration methodology to be effective during array

processing, the phase of the estimated calibrated signal should be accurate. Hence MSE in terms of phase error is analyzed in this paper. The MSE values are computed as

$$\text{MSE} = \frac{1}{K}\sum_{i=1}^{K}\left\|\angle\hat{C}_i - \angle C\right\|^2 \tag{19}$$

where $\angle\hat{C}_i$ and $\angle C$ are the phase values of the estimated and simulated calibration matrix, respectively, and K is the number of simulation runs.

From Figure 3, it can be observed that the proposed methodology is significantly sensitive to the input noise when $T < 100\,\text{ms}$. But the MSE of the estimated calibration parameters improves for longer coherent integration times. For further analysis, $T = 1\,\text{s}$ is considered. It is noted that in real scenarios, the data bits can be wiped-off using bit estimation algorithms exploiting for example the signal from the first antenna.

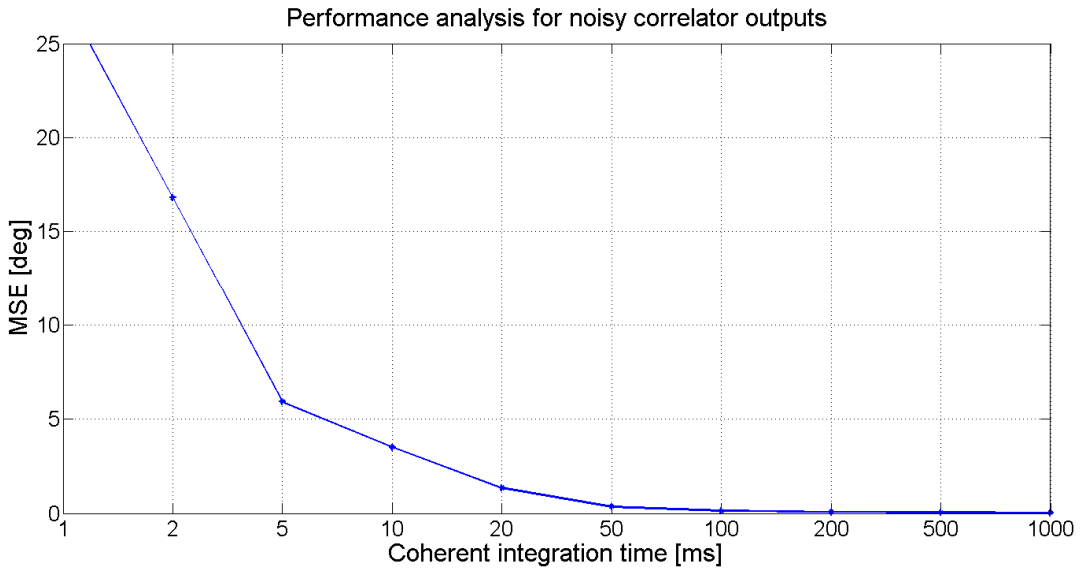

Figure 3 Phase mean square error of the projection based calibration algorithm as a function of the coherent integration time, *T*

Experimental Setup

In order to experimentally validate the effectiveness of the proposed calibration algorithm, several experiments were conducted using hardware simulated and real GPS signals. Two different data collection systems have been employed.

GPS signals were simulated using a Spirent GSS 7700 GPS hardware simulator capable of producing data from two separate antennas. The hardware simulator was used as an initial step before using real data. In this way, it was possible to test the proposed algorithm in a controlled environment where the impact of different factors such as antenna gain/phase mismatch and different hardware signal paths can be studied separately. Real data were then collected using up to 4 antennas.

Data were collected at first using a NI vector analyzer equipped with three PXI-5661 front-ends [20]. In this case, it was possible to collect data with up to three channels/antennas. The second acquisition system has been developed internally in the PLAN Group at the University of Calgary and it is an extension of the single channel front-end detailed in [9]. In this case, it was possible to collect data from up to 4 antennas. The PLAN Group acquisition system is shown in Figure 4 whereas the different typologies of experiments are summarized in Table 1.

The processing of multi-antenna data was performed using a modified version of the University of Calgary software receiver, GSNRx^{TM} [10] able to provide synchronous correlator outputs. The modified software, GSNRX^{TM}-rr, [21] is capable of tracking a reference channel and aiding several rover channels as shown in Figure 2 to produce correlator outputs according to (10). Here $\tilde{x}_0(t)$ is used as reference signal and $\tilde{x}_1(t), \tilde{x}_2(t), \cdots \tilde{x}_{M-1}(t)$ are fed to the rover processing channels. In order to reduce the

noise impact, a coherent integration time T = 1 s was adopted. Long coherent integration was achieved by estimating and removing the data bits using the reference signal from the first antenna.

In all cases, the proposed calibration algorithm was able to estimate the calibration parameters enabling DoA with an azimuth/elevation error within 10 degrees. In order to avoid the repetition of similar findings, only the experiments in the shaded cells of Table 1 are detailed in the following sections.

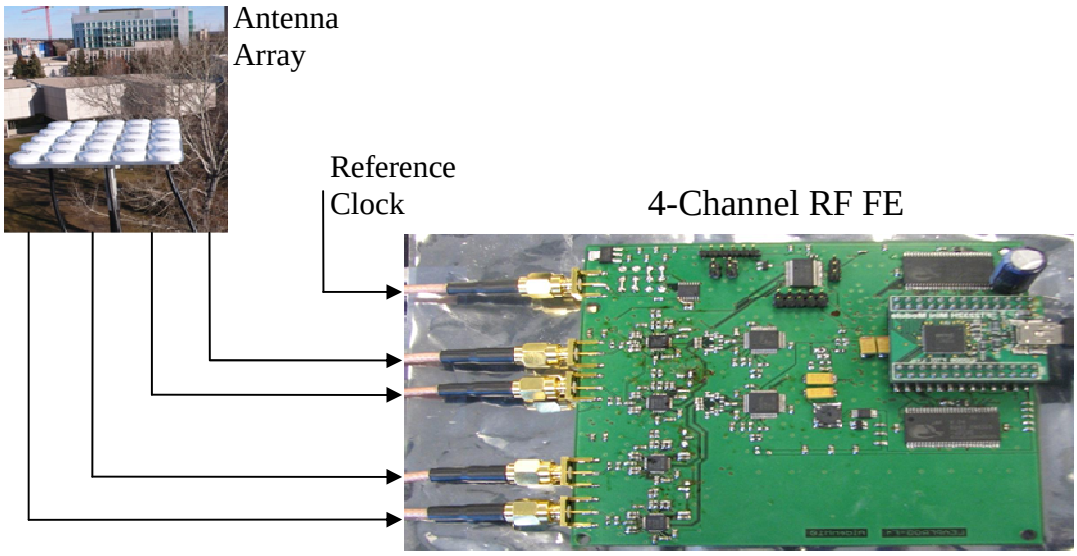

Figure 4 PLAN Group front-end able of synchronously acquiring data from up to 4 antennas

Table 1 Summary of the experiments performed for testing the proposed acquisition system

	NI data acquisition system	PLAN Group data acquisition system
Spirent GSS 7700 GPS hardware simulator	2 antennas	2 antennas
Live GPS Signals	Up to 3 antennas	Up to 4 antennas

Hardware Simulator Experiment

The test setup adopted when using the hardware simulator and the NI data acquisition system is shown in Figure 5 where Channel 1 and Channel 2 correspond to Antenna 1 and Antenna 2, respectively. The Spirent Hardware Simulator is able to provide signals from two channels (antennas) and thus only two front-ends were used.

The setup introduces a phase mismatch between channels due to the presence of different signal paths and front-ends used to collect data for further processing. This kind of setup allows the analysis of the calibration algorithm in the absence of mutual coupling.

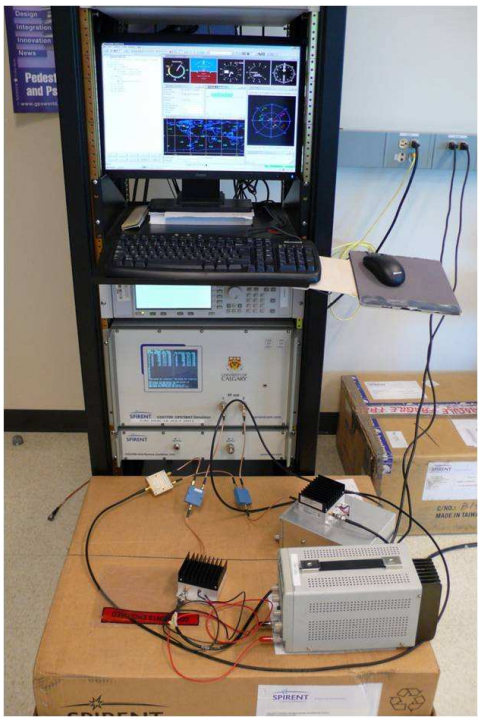

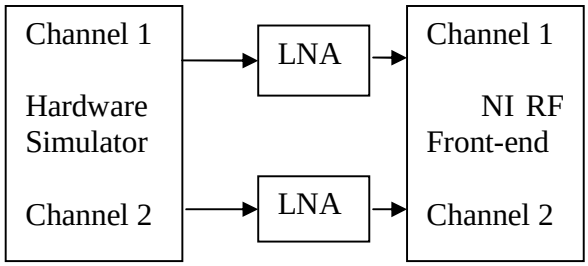

Parameters	Description
Sampling frequency	10 MHz Complex
Data Duration	5 min
L	10
M	2
Antenna Pattern	Isotropic NovAtel (702GG)

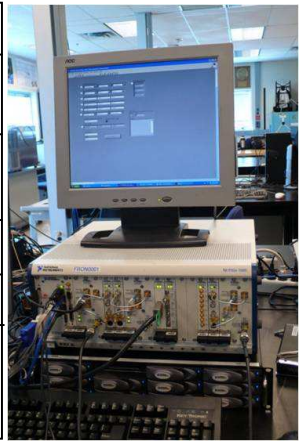

Figure 5 Data collection setup using a hardware simulator to provide dual channel data.

The front-ends used for the data collection were driven by the same clock; however since two different PLLs were used for the signal down-conversion, it was not possible to

guarantee phase coherence among the channels. Thus, even after calibration, a relative phase drift was observed between the signal components of the two channels.

In order to compensate for relative phase variations along time among different front-ends, a reference sine wave was combined with the simulator data. This pilot tone was used to estimate the phase drift between channels. Details relative to the algorithm used for compensating phase changes can be found in [22]. It is noted that the relative phase drift problem is essentially due to the fact that the NI system was not designed for array processing and this problem is not present when the PLAN Group front-end is used. For this reason the issue is not further discussed. In the following figure, the effect of phase drift between channels has been removed and only the effect of the calibration procedure is highlighted.

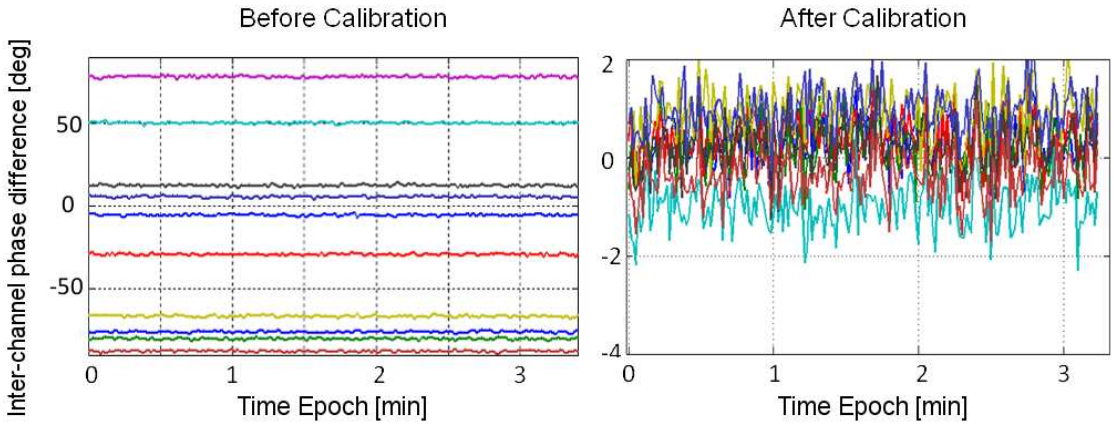

Figure 6 Phase difference between signals from two different channels before and after calibration. The effect of the steering vector has been removed in both cases. After calibration and steering vector removal, signals from different channels are in phase. Hardware simulator experiment.

Results obtained using the hardware simulator and the NI system is shown in Figure 6.

More specifically, Figure 6 shows the phase difference between signals from the hardware simulator channels before and after calibration. In both cases, the effect of the steering vector has been removed. After correcting for the calibration parameters and removing the phase terms due to the steering vector, all the signals from the same satellite are properly aligned in phase allowing beamforming. Only after calibration, signals from different antennas can be coherently combined on the basis of the steering vector information. This type of plot is preferred here to the array factor graphs used in the next section for real-data analysis because of the limed number (only two) of channels used for the demonstration. When only two antennas are used the array factor is characterized by large bands and the effect of calibration is not clearly observable. The results shown in Figure 6 support the effectiveness of the proposed algorithm that enable array processing even in particularly adverse conditions such as that obtained using the NI data collection system.

Real data analysis

In order to further test the proposed calibration technique, live data from GPS satellites were used. Four antennas were spaced 6 cm apart in a planar structure as shown in Figure 7 and data were synchronously collected using the PLAN Group front-end described above. It should however be noted that the array is non-traditional and is used in this research work only for demonstrating the proposed calibration algorithm. The array is non-traditional, in the sense that no effort was made in minimizing mutual coupling and commercially available antennas were directly mounted on a rigid structure. Similarly, data were collected using a triangular array structure to analyze the performance of

calibration for varying array configurations as shown in Figure 7. Here A0-A3 represents locations of different antennas used to form the planar/triangular structure.

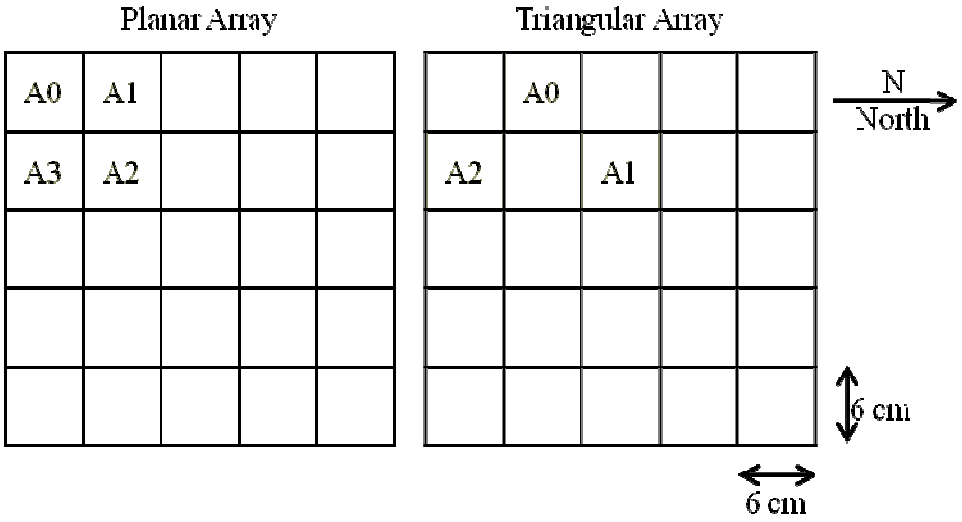

Figure 7 Placement of antennas in planar and triangular structures on the 5x5 grid used for the real data collection.

Figure 8 shows sample beamforming results for two different satellites not considered for calibration procedure, SV-ID 3 and SV-ID 22 with elevation angles 21° and 80°, respectively. The figure shows the gain provided by the array after applying beamforming as a function of azimuth and elevation. The plot has been produced considering the array pattern parameters provided in [19]. It can be observed that before calibration, the array beam pattern maximum is away from the true direction of arrival (denoted by 'x'). After applying the proposed projection based calibration methodology, the array beam pattern has a maximum around the true direction of arrival for both satellites. Similar results have been observed for the other satellites in view.

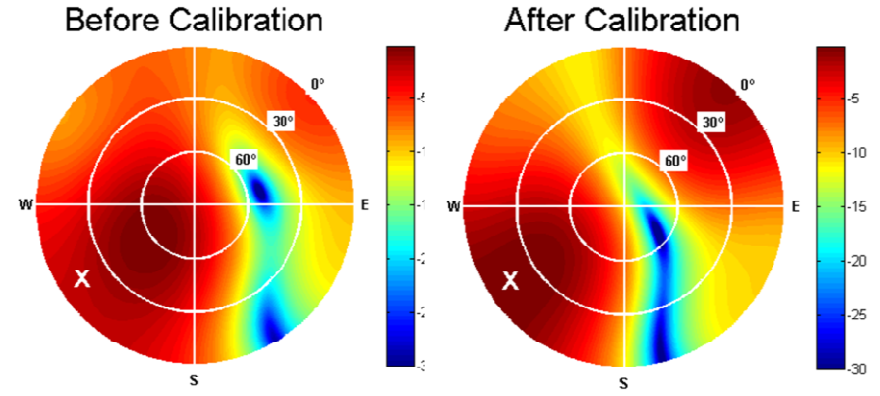

SVID 3: $\alpha = 236^{\circ}, \epsilon = 21^{\circ}$

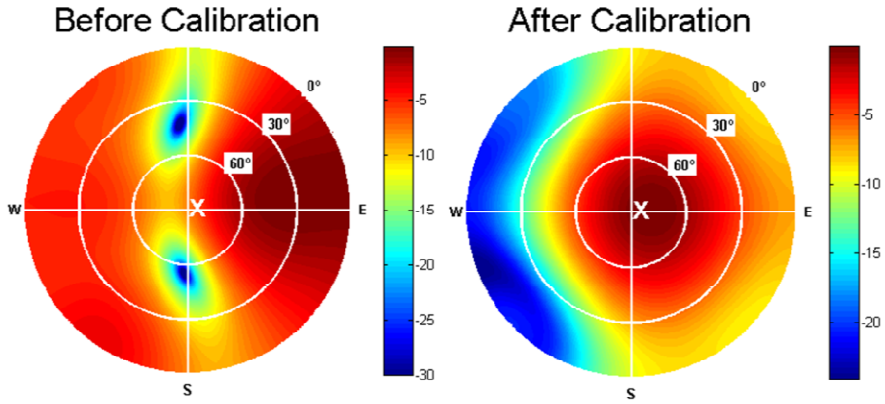

SVID 22: $\alpha = 72^{\circ}, \epsilon = 80^{\circ}$

Figure 8 Real data beamforming results before and after applying the projection based calibration methodology on planar array data. The beamforming values provided in dB are relative to the peak response.

To further analyze the effect of calibration errors on real data beamforming, angular errors on the estimated elevation and azimuth angles has been evaluated. Angular error represents the difference between estimated and true Azimuth/Elevation angle. The results for the angular errors in azimuth and elevation for the different satellites in view are provided in Figure 9 and Figure 10, respectively. The plots in Figure 9 and Figure 10 provide angular errors obtained after applying beamforming on calibrated array outputs

for different GPS satellites. The angular error, ϵ_θ^i, has been computed for both elevation and azimuth angles using the formulation:

$$\epsilon_\theta^i = \theta_{TDOA}^i - \theta_{BDOA}^i \tag{19}$$

where θ_{TDOA}^i is the true direction of arrival of the incoming signal computed using the ephemeris collected from the reference antenna and θ_{BDOA}^i is the direction of arrival that maximizes the energy of the correlator outputs combined through beamforming at the i^{th} instant in time. This kind of analysis provides a means to analyse the effect of residual calibration errors on array processing algorithms.

From Figure 9, the azimuth error along time is observed to be within ±10 degrees for most of the satellites considered.

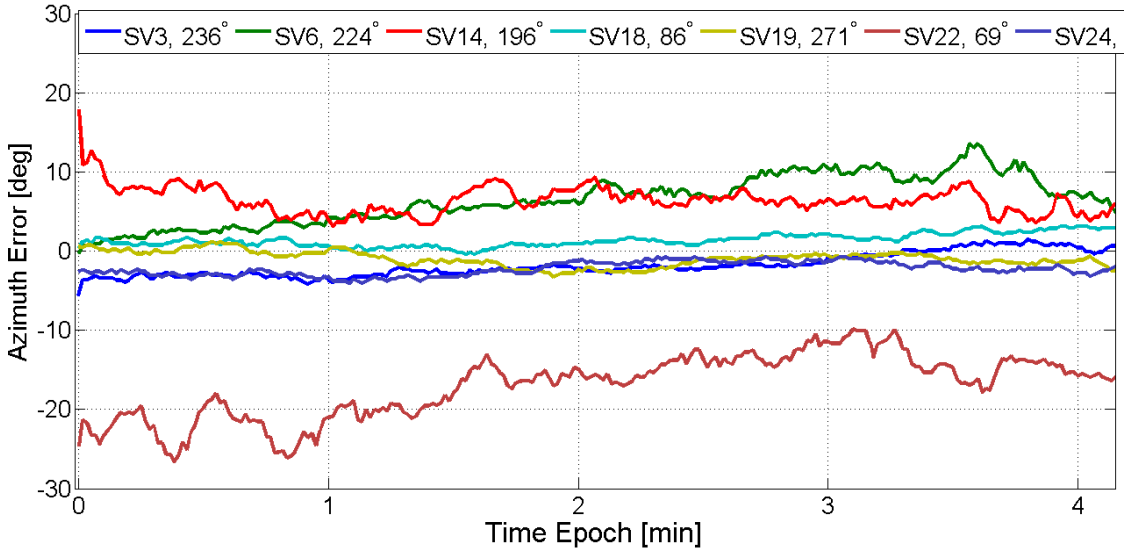

Figure 9 Azimuth errors after performing angle of arrival estimation on the calibrated planar array data.

It is noted that, since only 4 antennas are used, the beam of the array is quite wide leading to a poor resolution in the azimuth domain. This is the case of SV-ID 22 (large errors due

to the fact that satellite is at zenith where small changes in DoA results in large changes in azimuth angle) that has a larger error as compared to the other satellites. It can be observed from Figure 10 that the elevation error along time is within ±5 degrees for high elevation satellite signals (SV-ID 14, 18, 19 and 22) and around ±10 degrees for medium-to-low elevation angles (SV-ID 3, 6, 24). In these plots, calibration was performed only once at the start of the data set. These results support the effectiveness of the proposed algorithm that enables beamforming algorithms. Without calibration, angle of arrival estimation was simply not possible.

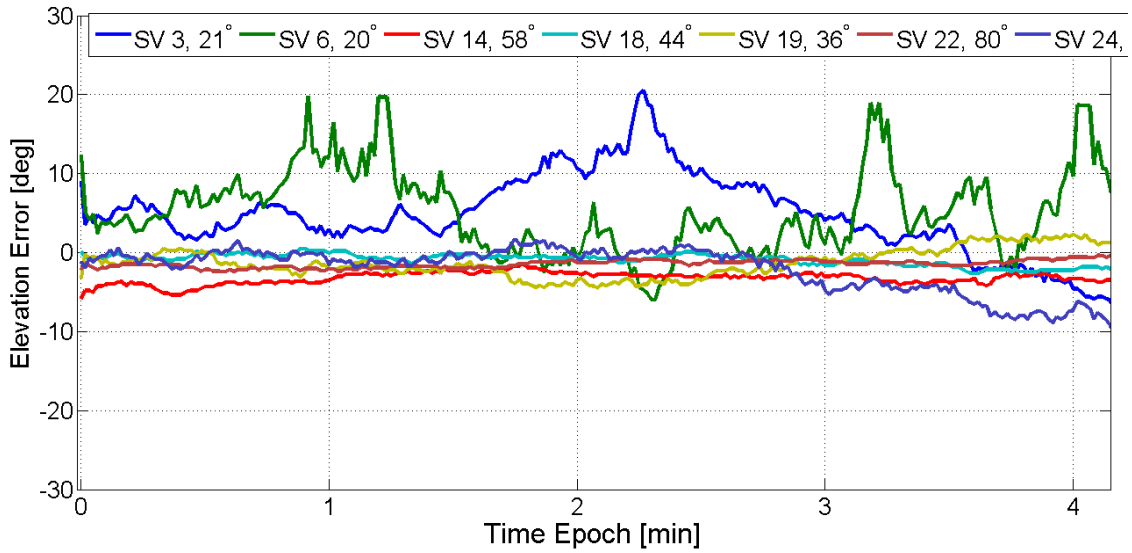

Figure 10 Elevation errors after performing angle of arrival estimation on the calibrated planar array data.

Sample results on beamforming for triangular array data after applying the projection based calibration methodology are provided in Figure 11 for two different satellites. It should be noted that since only three antennas are considered, the main lobe of the array

pattern is wider as compared to the array beam pattern obtained in Figure 8 where four antennas were considered.

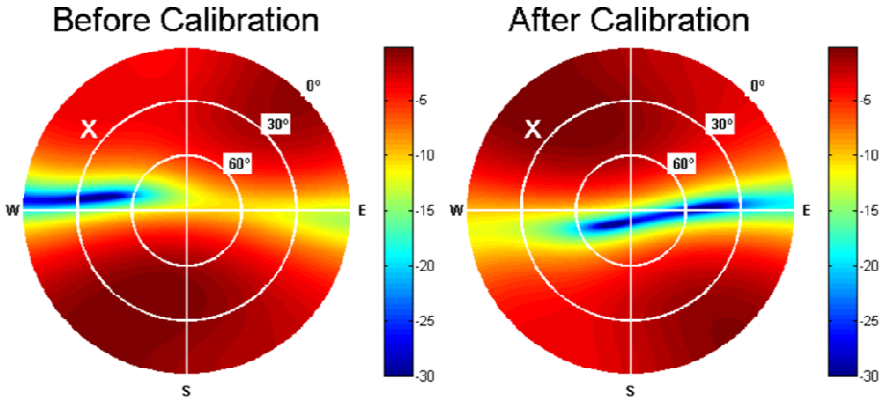

SVID 3: $\alpha = 314^{\circ}, \epsilon = 23^{\circ}$

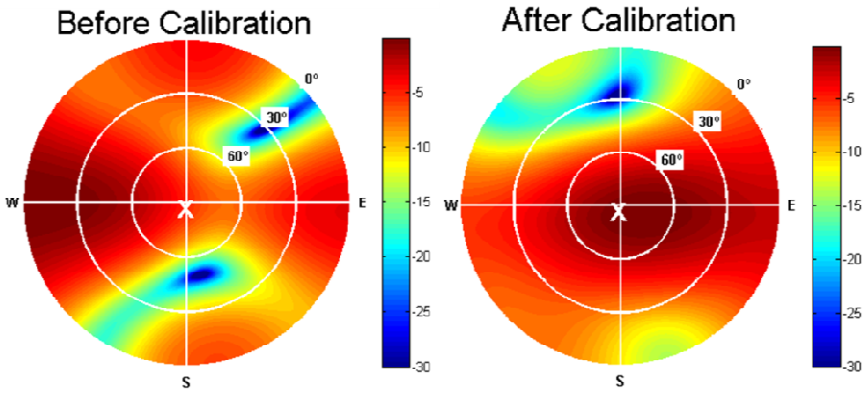

SVID 22: $\alpha = 114^{\circ}, \epsilon = 85^{\circ}$

Figure 11 Real data beamforming results before and after applying projection based calibration methodology on triangular array data. The beamforming values provided in dB are relative to the peak response.

From Figure 11, it can be observed that calibration maximizes the array beam pattern around the true direction of arrival (denoted by 'x') for the considered satellites. Thus, in both planar and triangular array structures, the proposed calibration algorithm was able to provide calibrated correlator outputs that maximize the incoming signal power around the true direction of arrival.

CONCLUSIONS

A self-contained antenna array calibration procedure using GNSS signals has been proposed and analyzed. The algorithm exploits the properties of the signal steering vector and accounts for signal gain/phase mismatches and mutual coupling between antenna elements. The proposed algorithm is able to effectively calibrate the antenna array without requiring any additional equipment for the generation of signal from sources at known positions, enabling for inline calibration of GNSS receivers adopting multiple antennas. The technique has been tested with simulations and real data. Two different hardware systems have been used for the data collections and consistent results have been obtained in the different cases. Experiments using live GPS data show the feasibility of the proposed algorithm and support its effectiveness in enabling multi-antenna processing for beamforming and DoA applications. Additional work is required for verifying and extending the suitability of the proposed algorithm to other applications.

References

[1] Balanis, C. A. and P. Ioannides *Introduction to Smart Antennas*, Synthesis Lectures on Antennas #5, Morgan & Claypool Publishers' Series, pp. 33-67, ISBN 1598291769, 2007

[2] Gupta, I. J., J. R. Baxter, S. W. Ellingson, H. G. Park, H. S. Oh, and M. G. Kyeong "An experimental study of antenna array calibration," in *IEEE Transactions on Antennas and Propagation*, Vol. 51, March 2003, pp. 664-667

[3] Ng, B. C. and C. M.S. See "Sensor-Array Calibration Using a Maximum-Likelihood Approach," *IEEE Transactions on Antennas and Propagation*, vol. 44, no. 6, June 1996, pp. 827-835

[4] Backen, S., D. M. Akos, and M. L. Nordenvaad "Post-Processing Dynamic GNSS Antenna Array Calibration and Deterministic Beamforming," in *Proceedings of the 21st International Tecnical Meeting of the Satellite Division*, 16-19 September 2008, Savannah, GA, The Institute of Navigation, pp. 2806-2814

[5] Church, C. M. and I. J. Gupta "Calibration of GNSS Adaptive Antennas," in *Proceedings of the 22nd International Meeting of the Satellite Division of The Institute of Navigation*, 22-25 September 2009, Savannah, GA

[6] Schmidt, R. O. "Multiple Emitter Location and Signal Parameter Estimation," in *IEEE Transactions on Antennas and Propagation*, Vol. 34, Issue 3, March 1986 1986, pp. 276-280

[7] Park, H. G. and S. C. Bang "Model based antenna array calibration for digital beamforming systems," in *Proceedings of the 57th IEEE Semiannual Vehicular Technology Conference*, Spring 2003, pp. 867

[8] NI (2006) *2.7 GHz RF Vector Signal Analyzer with Digital Downconversion, National Instruments*, http://www.ni.com/pdf/products/us/cat_vectorsignalanalyzer.pdf

[9] Morrison, A. *GNSS Signal Tracking Methods Under Ionospheric Scintillation*, PhD Thesis, published as Report No. 20312, The University of Calgary, 2010

[10] Petovello, M. G., C. O'Driscoll, G. Lachapelle, D. Borio, and H. Murtaza "Architecture and Benefits of an Advanced GNSS Software Receiver," *Positioning*, vol. 1, no. 1, August 2009, pp. 66-78

[11] Anantharamu, P. B., D. Borio, and G. Lachapelle "Self-contained GNSS-based Antenna Array Calibration," in *Proceedings of the 2011 International Technical Meeting of The Institute of Navigation*, 24 - 26 January 2011, San Diego, pp. 1232 - 1239

[12] Gupta, I. J. and A. A. Ksienski "Effect of Mutual Coupling on the Performance of Adaptive Arrays," in *IEEE Transactions on Antennas and Propagation*, Vol. AP-31, Issue 5, 1983, pp. 785-792

[13] Kaplan, E. D. and C. J. Hegarty *Understanding GPS Principles and Applications*, Artech House, pp. 155-200, ISBN-13:978-1-58053-894-7, 2006

[14] Teunissen, P. J., G. G. N. Nadarajah, and P. J. Buist "Low-Complexity Instantaneous GNSS Attitude Determination with Multiple Low-Cost Antennas," in *Proceedings of the Proceedings of the 24th Internationsl Technical Meeting of the Satellite Division of the Institute of Navigation (ION GNSS 2011)*, 2011, Portland, OR, pp. 3874-3880

[15] Trefethen, L. N. and D. Bau *Numerical linear algebra*, Society for Industrial and Applied Mathematics, Philadelphia, pp. 56-61, ISBN 0-89871-361-7, 1997

[16] Mikhail, E. M. *Observations and least squares* , Intext Educational Publishers, New York, pp. 497, ISBN 0700224815, 1976

[17] Van Veen, B. D. and K. M. Buckley "Beamforming: a versatile approach to spatial filtering," *IEEE ASSP Magazine*, vol. 5, no. 2, April 1988, pp. 4-24

[18] Tranter, W. H., K. S. Shanmugan, T. S. Rappaport, and K. L. Kosbar *Principles of Communication Systems Simulation with Wireless Applications*, Prentice Hall, Communications Engineering and Emerging Technologies Series, 2004

[19] Kunysz, W. "A Novel GPS Survey Antenna," in *Proceedings of the Institute of Navigation NTM 2000*, 26-28 January 2000, Anaheim, CA, pp. 698-705

[20] Borio, D. (2010) *GNSS Receiver Design*, ENGO 638 Course Notes, Department of Geomatics Engineering, University of Calgary, Canada

[21] Satyanarayana, S., D. Borio, and G. Lachapelle "Power Levels and Seconds Order Statistics for Indoor fading Using a Calibrated A-GPS Software Receiver," in *Proceedings of the ION GNSS10*, 21-24 September 2010, Portland

[22] Anantharamu, P. B. *Space-Time Equalization Techniques for New GNSS Signals*, PhD Thesis, University of Calgary, 2011 (Available at http://plan.geomatics.ucalgary.ca/)